

Spatial interference between pairs of disjoint optical paths with a single chaotic source

Michele Cassano¹, Milena D'Angelo^{1,2}, Augusto Garuccio^{1,2}, Tao Peng^{3,4}, Yanhua Shih,³ and Vincenzo Tamma ^{*5,6}

¹Dipartimento Interateneo di Fisica, Università degli Studi di Bari, 70100 Bari, Italy

²Istituto Nazionale Di Fisica Nucleare, sez. di Bari, 70100 Bari, Italy

³Department of Physics, University of Maryland, Baltimore County, Baltimore, MD 21250, USA

⁴Institute for Quantum Science and Engineering, Texas A & M University, College Station, Texas 77843, USA

⁵Institut für Quantenphysik and Center for Integrated Quantum Science and Technology (IQST), Universität Ulm, D-89069 Ulm, Germany

⁶Faculty of Science, SEES, University of Portsmouth, Portsmouth PO1 3QL, UK

March 2, 2022

Abstract

We demonstrate a novel second-order spatial interference effect between two indistinguishable pairs of disjoint optical paths from a *single* chaotic source. Beside providing a deeper understanding of the physics of multi-photon interference and coherence, the effect enables retrieving information on both the spatial structure and the relative position of two distant double-pinhole masks, in the absence of first order coherence. We also demonstrate the exploitation of the phenomenon for simulating quantum logic gates, including a controlled-NOT gate operation.

OCIS codes: (030.0030) Coherence and statistical optics; (120.3180) Interferometry; (270.0270) Quantum optics.

References

- [1] R. Hanbury Brown and R.Q. Twiss, “Correlation between photons in two coherent beams of light,” *Nature* **177**, 27 - 29 (1956).
- [2] R. Hanbury Brown and R.Q. Twiss, “A test of a new type of stellar interferometer on sirius,” *Nature* **178**, 1046 -1048 (1956).
- [3] R.J. Glauber, “Photon correlations,” *Phys. Rev. Lett.* **10**, 84 (1963).
- [4] R.J. Glauber, “One hundred years of light quanta,” Nobel Lecture 8 Dec 2005, (The Nobel Foundation 2005).

*vincenzo.tamma@port.ac.uk

- [5] C.O.Alley and Y.H.Shih *Proceedings of the Second International Symposium on Foundations of Quantum Mechanics in the Light of New Technology* ed of Japan P S (Tokyo, 1986), pp 47 - 52; Y. H. Shih and C. O. Alley, “New type of Einstein-Podolsky-Rosen-Bohm experiment using pairs of light quanta produced by optical parametric down conversion,” *Phys. Rev. Lett.* **61**, 2921 (1988).
- [6] C. K. Hong, Z. Y. Ou, and L. Mandel, “Measurement of subpicosecond time intervals between two photons by interference,” *Phys. Rev. Lett.* **59**, 2044 (1987).
- [7] H. Kim, O. Kwon, W. Kim, and T. Kim, “Spatial two-photon interference in a Hong-Ou-Mandel interferometer,” *Phys. Rev. A* **73**, 023820 (2006).
- [8] J. Liu, Y. Zhou, W. Wang, R.F. Liu, K. He, F.L. Li, and Z. Xu, “Spatial second-order interference of pseudothermal light in a Hong-Ou-Mandel interferometer,” *Optics Express* **21**(16), 19209 - 19218 (2013).
- [9] V. Tamma and S. Laibacher, “Multiboson correlation interferometry with multimode thermal sources,” *Phys. Rev. A* **90**, 063836 (2014).
- [10] V. Tamma and S. Laibacher, “Multiboson correlation interferometry with arbitrary single-photon pure states” *Phys. Rev. Lett.* **114**, 243601 (2015).
- [11] V. Tamma and J. Seiler, “Multipath correlation interference and controlled-not gate simulation with a thermal source,” *New J. Phys.* **18**, 032002 (2016).
- [12] M. Genovese “Real applications of quantum imaging,” *Journal of Optics* **18**(7), 073002 (2016).
- [13] M. D’Angelo, M.V. Chekhova, and Y.H. Shih, “Two-photon diffraction and quantum lithography,” *Phys. Rev. Lett.* **87**, 013602 (2001).
- [14] G.B. Lemos, V. Borish, G.D. Cole, S. Ramelow, R. Lapkiewicz, and A. Zeilinger, “Quantum imaging with undetected photons,” *Nature* **512**, 409–412 (2014).
- [15] J. Sprigg, T. Peng, and Y.H. Shih, “Super-resolution imaging using the spatial-frequency filtered intensity fluctuation correlation,” *Scientific Reports* **6**, 38077 (2016).
- [16] T.B. Pittman, Y.H. Shih, D.V. Strekalov, and A.V. Sergienko, “Optical imaging by means of two-photon quantum entanglement,” *Phys. Rev. A* **52**, R3429 (1995).
- [17] A. Valencia, G. Scarcelli, M. D’Angelo, and Y.H. Shih “Two-photon imaging with thermal light,” *Phys. Rev. Lett.* **94**, 063601 (2005).
- [18] M. D’Angelo and Y.H. Shih, “Quantum Imaging,” *Laser Phys. Lett.* **2**(12), 567 - 596 (2005).
- [19] G. Scarcelli, V. Berardi, and Y.H. Shih, “Can two-photon correlation of chaotic light be considered as correlation of intensity fluctuations?,” *Phys. Rev. Lett.* **96**, 063602 (2006).
- [20] A. Gatti, E. Brambilla, M. Bache, and L. A. Lugiato, “Correlated imaging, quantum and classical,” *Phys. Rev. A* **70**, 013802 (2004).
- [21] F. Ferri, D. Magatti, A. Gatti, M. Bache, E. Brambilla, and L. A. Lugiato, “High-resolution ghost image and ghost diffraction experiments with thermal light,” *Phys. Rev. Lett.* **94**, 183602 (2005).
- [22] H. Chen, T. Peng, and Y.H. Shih, “100% correlation of chaotic thermal light,” *Phys. Rev. A* **88**, 023808 (2013).
- [23] K.-H. Luo, B.-Q. Huang, W.-M. Zheng and L.-A. Wu “Nonlocal Imaging by Conditional Averaging of Random Reference Measurements,” *Chin. Phys. Lett.* **29**(7), 074216 (2012).
- [24] P. Kok, “Photonic quantum information processing,” *Contemporary Physics* **57**(4), 526 - 544 (2016).
- [25] M. Nielsen and I. Chuang *Quantum Computation and Quantum Information* (Cambridge Series on Information and the Natural Sciences, Cambridge University Press, 2000).

- [26] V. Tamma, “Sampling of bosonic qubits,” *International Journal of Quantum Information* **12**, 1560017 (2014).
- [27] S. Laibacher and V. Tamma, “From the physics to the computational complexity of multiboson correlation interference,” *Phys. Rev. Lett.* **115**, 243605 (2015).
- [28] V. Tamma V. and S. Laibacher S., “Boson sampling with non-identical single photons,” *Journ. of Mod. Opt.* **63**(1), 41 - 45 (2016).
- [29] V. Tamma and S. Laibacher, “Multi-boson correlation sampling,” *Quantum Inf. Process.* **15**(3), 1241 - 1262 (2016).
- [30] V. Giovannetti, S. Lloyd, and L. Maccone, “Advances in quantum metrology,” *Nature Photonics* **5**(4), 222-229 (2011).
- [31] V. Giovannetti, S. Lloyd, and L. Maccone, “Quantum-Enhanced Measurements: Beating the Standard Quantum Limit,” *Science* **306**(5700), 1330-1336 (2004).
- [32] J. Dowling, “Quantum optical metrology - the lowdown on high-N00N states,” *Contemporary Physics* **49**(2), 125 - 143 (2008).
- [33] T. Legero, T. Wilk, M. Hennrich, G. Rempe, and A. Kuhn, “Quantum Beat of Two Single Photons,” *Phys. Rev. Lett.* **93**, 070503 (2004).
- [34] M. D’Angelo, A. Garuccio, and V. Tamma, “Toward real maximally path-entangled N -photon-state sources,” *Phys. Rev. A* **77**, 063826 (2008).
- [35] N. Cerf, C. Adami, and P. Kwiat, “Optical simulation of quantum logic,” *Phys.Rev. A* **57**, R1477 (1998).
- [36] R.J.C. Spreeuw, “Classical wave-optics analogy of quantum-information processing,” *Phys. Rev. A* **63**, 062302 (2001).
- [37] K.F. Lee and J.E. Thomas, “Experimental simulation of two-particle quantum entanglement using classical fields,” *Phys. Rev. Lett.* **88**, 097902 (2002).
- [38] K.H. Kagalwala, G. di Giuseppe, A.F. Abouraddy and B.E.A. Saleh, “Bell’s measure in classical optical coherence,” *Nature Photonics* **7**(1), 72 - 78 (2013).
- [39] T. Peng and Y.H. Shih, “Bell correlation of thermal fields in photon-number fluctuations,” *EPL* **112**(6), 60006 (2015).
- [40] I. N. Agafonov, M. V. Chekhova, T. S. Iskhakov, and L.-A. Wu, “High-visibility intensity interference and ghost imaging with pseudo-thermal light,” *Journ. of Mod. Opt.* **56**(2-3), 422 - 431 (2009).
- [41] M. E. Pearce, T. Mehringer, J. von Zanthier, and P. Kok, “Precision estimation of source dimensions from higher-order intensity correlations,” *Phys. Rev. A* **92**, 043831 (2015).
- [42] G. Scarcelli, A. Valencia, and Y.H. Shih, “Two-photon interference with thermal light,” *EPL* **68**(5), 618 - 624 (2004).
- [43] S. Oppel, T. Büttner, P. Kok, and J. von Zanthier, “Superresolving multiphoton interferences with independent light sources,” *Phys. Rev. Lett.* **109**, 233603 (2012).
- [44] T.B. Pittman , M.J. Fitch, B.C. Jacobs, and J.D. Franson, “Experimental controlled-NOT logic gate for single photons in the coincidence basis,” *Phys. Rev. A* **68**, 032316 (2003).
- [45] J.L. O’Brien, G.J. Pryde, A.G. White, T.C. Ralph, and D. Branning, “Demonstration of an all-optical quantum controlled-NOT gate,” *Nature* **426**, 264 - 267 (2003).
- [46] K. Sanaka, K. Kawahara, and T. Kuga, “Experimental probabilistic manipulation of down-converted photon pairs using unbalanced interferometers,” *Phys. Rev. A* **66**, 040301 (2002).

- [47] M. D’Angelo, A. Mazzilli, F. V. Pepe, A. Garuccio, and V. Tamma V., “Characterization of two distant double-slit by chaotic light second-order interference,” arxiv: 1609.03416 (2016).
- [48] T. Peng, V. Tamma, and Y.H. Shih, “Experimental controlled-not gate simulation with thermal light,” *Scientific Reports* **6**, 30152 (2016).
- [49] R.J. Glauber *Quantum Theory of Optical Coherence: Selected Papers and Lectures* (John Wiley and Sons, 2007).
- [50] L. Mandel and E. Wolf *Optical Coherence and Quantum Optics* (Cambridge University Press, 1995).
- [51] E.C.G. Sudarshan, “Equivalence of semiclassical and quantum mechanical description of statistical light beams,” *Phys. Rev. Lett.* **10**, 277 (1963).
- [52] A. Crespi, M. Lobino, J.C.F. Matthews, A. Politi, C.R. Neal, R. Ramponi, R. Osellame, and J.L. O’Brien, “Measuring protein concentration with entangled photons,” *Appl. Phys. Lett.* **100**(23), 233704 (2012).
- [53] V. Tamma, “Analogue algorithm for parallel factorization of an exponential number of large integers: II. optical implementation,” *Quantum Information Processing* **15**(12), 5243 - 5257 (2015).
- [54] V. Tamma, “Analogue algorithm for parallel factorization of an exponential number of large integers: I. theoretical description,” *Quantum Information Processing* **15**(12), 5259 - 5280 (2015).
- [55] V. Tamma, H. Zhang, X. He, A. Garuccio, W.P. Schleich, and Y.H. Shih, “Factoring numbers with a single interferogram,” *Phys. Rev. A* **83**, 020304 (2011).
- [56] V. Tamma, H. Zhang, X. He, A. Garuccio, and Y.H. Shih, “New factorization algorithm based on a continuous representation of truncated gauss sums,” *Journ. of Mod. Opt.* **56**(18), 2125 - 2132 (2009).
- [57] V. Tamma, C.O. Alley, W.P. Schleich, and Y.H. Shih, “Prime Number Decomposition, the Hyperbolic Function and Multi-Path Michelson Interferometers,” *Foundations of Physics* **42**(1), 111 - 121 (2012).
- [58] S. Wölk, W. Merkel, W.P. Schleich, I.S. Averbukh, and B. Girard, “Factorization of numbers with Gauss sums: I. Mathematical background,” *New J. Phys.* **13**, 103007 (2011).
- [59] Y.H. Shih *An Introduction to Quantum Optics* (CRC Press Taylor and Francis group, 2011).
- [60] M.H. Rubin, “Transverse correlation in optical spontaneous parametric down-conversion,” *Phys. Rev. A* **54**, 6 (1996).

1 Introduction

The second-order interference phenomena investigated in the mid-1950s by Hanbury Brown and Twiss (HBT) imposed a deep change in the understanding of interference and coherence [1, 2]. In fact, the intense debate raised by HBT interferometry naturally led to the development of quantum optics [1, 2, 3, 4], with its intriguing fundamental studies on multi-photon interference [5, 6, 7, 8, 9, 10, 11], its promising applications (e.g., imaging [13, 14, 15, 16, 17, 18, 19, 20, 21, 22, 23, 12], quantum information processing [24, 25, 26, 27, 28, 29], metrology [30, 31, 13, 32], etc.), and developments (e.g., N-photon state characterization [10, 33], entanglement generation [10, 34] and entanglement simulation [35, 36, 37, 38, 39]).

In the original HBT interferometer [1], second order interference is observed when light emitted by a single chaotic source is detected by two separate sensors and correlation measurements are performed while varying either the time delay between the two detectors (temporal second-order interference) or their relative position (spatial second-order interference). The two detectors, separately, do not retrieve any (first-order) interference. However, interference is observed at second-order provided the time delay and the spatial separation are within the coherence time and the coherence area of the source, respectively.

Recently, Tamma and Seiler have proposed a modification of this scheme [11]: before reaching the detectors, chaotic light propagates through two unbalanced M-Z interferometers. No first-order interference exists at the exit of the interferometers, since the unbalancing is larger than the coherence length of the source. Interestingly, interference between two long and two short paths is predicted to occur even if the relative time-delay between the two pairs is beyond the coherence time of the source. This interferometer, substantially different from previous schemes based on multiple incoherent sources [40, 41, 42, 43], thus offers a deeper insight on the interplay between interference and coherence in multiphoton interferometry. Furthermore, a controlled-NOT (CNOT) gate operation [44, 45, 46] can be simulated by employing this interference effect [11].

In this paper, we demonstrate that pure second-order interference between pairs of disjoint optical paths (paths which do not overlap spatially), originated from a single chaotic source, can also be observed in the spatial domain. The uniqueness of such a spatial interference phenomenon stands in its potential application for sensing of remote objects. In particular, we consider an optical interferometer (Fig. 1) where the light from a single chaotic source, after being split by a balanced beam splitter, propagates through two double-pinhole masks placed in the two separate output channels of the beam splitter. The separation between the pinholes in each mask is such that no first-order interference can be observed by the detectors placed behind each mask. However, as shown in Section 2, by measuring the correlation between the photon number fluctuations at given transverse positions of the two detectors, a spatial second-order interference is predicted to appear. Interference occurs between two pairs of disjoint optical paths, which are defined by the two pairs of pinholes $(1_C, 1_T)$ and $(2_C, 2_T)$. In Section 3, we show that the information about the spatial structure and the relative position of the two masks is encoded within the relative phase between the two pairs of interfering paths, independently of the distance between the two masks and the source. In particular, we demonstrate that: 1) this information can be retrieved in suitable experimental scenarios (Tables 1 and 2); 2) the measurement precision can be increased by changing some experimental parameters rather than increasing the frequency of the light (Table 1 and Fig. 2). Finally, in Section 4, we show that the proposed interference phenomenon can also be used to simulate quantum logic operations, including a CNOT gate.

The novel spatial interference effect introduced in this paper has already triggered two experiments: 1) the experimental characterization of two remote double-slit masks within the experimental scenarios (v) in Table 1, and (i), (ii) in Table 2 [47]; 2) the experimental simulation of the CNOT-gate operation based on the spatial interferometer introduced in Fig. 3 [48]. The more general results reported here provide the complete physical picture of the novel interference effect, and are likely to inspire further theoretical and experimental works (e.g., monitoring the relative change in the spatial structure of two distant masks, as predicted in Fig. 2). Intriguing applications in imaging and sensing of remote objects are in fact at reach with the current technology.

2 Spatial interference effect

Let us start by introducing the interferometric setup depicted in Fig. 1: chaotic light emitted by the source S is split by a balanced non-polarizing beam splitter, and two double-pinhole masks are placed in the output ports of the beam splitter, at the same distance z from the source. The pinholes are indicated as $1_C, 2_C$ for the upper mask and $1_T, 2_T$ for the lower mask. The light transmitted by the masks reaches two point-like detectors, D_C and D_T , placed at the same distance f from the masks. A correlation measurement is performed between the fluctuations of the number of photons detected by D_C and D_T .

We first consider the correlation in the number of photons on the masks planes, which is given by the second-order correlation function [49, 22]

$$G^{(2)}(x_p, x_q) \propto \langle n(x_p)n(x_q) \rangle = \langle n(x_p) \rangle \langle n(x_q) \rangle + \langle \Delta n(x_p) \Delta n(x_q) \rangle, \quad (1)$$

with $p = 1_C, 2_C$ and $q = 1_T, 2_T$, where n represents the photon number and $\Delta n := n - \bar{n}$ the photon-number fluctuation around the mean \bar{n} . In particular, we consider the case of a quasi-monochromatic chaotic source, which, for simplicity, is also assumed to be 1 dimensional and linearly polarized (e.g., along the horizontal H direction). The input chaotic light is described by [49, 50]

$$\hat{\rho}_H = \int \left[\prod_{\kappa} d^2 \alpha_{\kappa, H} \right] P(\{\alpha_{\kappa, H}\}) \bigotimes_{\kappa} |\alpha_{\kappa, H}\rangle_S \langle \alpha_{\kappa, H}|, \quad (2)$$

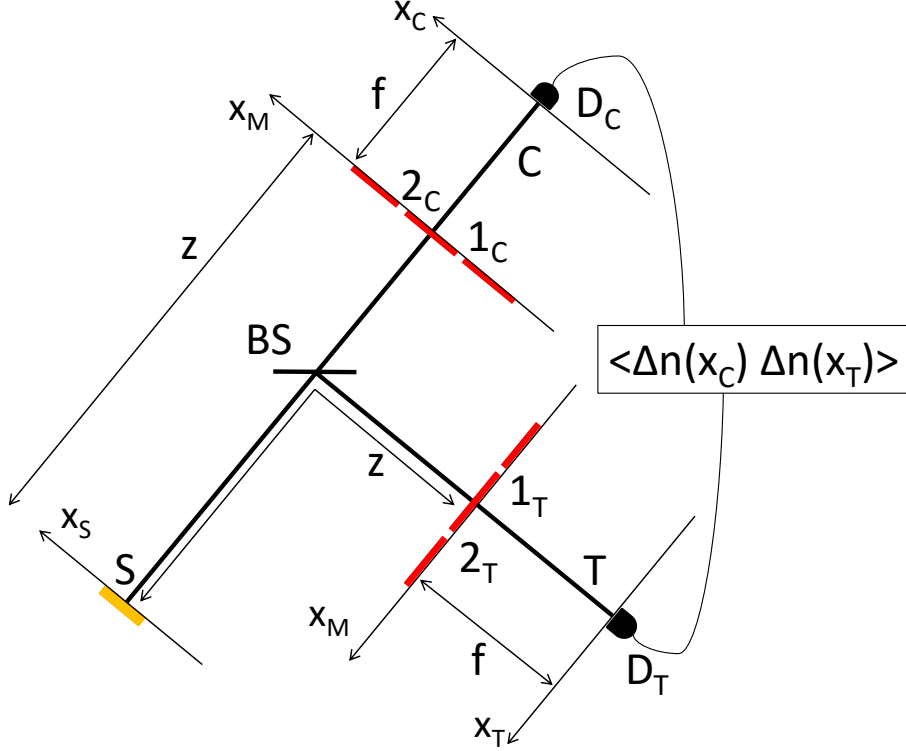


Figure 1: Optical interferometer for sensing two remote double-pinhole masks through the observation of spatial second-order interference between indistinguishable pairs of disjoint optical paths. Light emitted by a single 1 dimensional chaotic source, after being split by a balanced non-polarizing beam splitter, propagates through two double-pinhole masks placed at the same distance z from the source and reaches two point-like detectors, D_C and D_T , placed at distance f from the masks. A correlation measurement between the fluctuations of the number of photons at the detectors D_C and D_T is performed.

with the Glauber-Sudarshan probability distribution [3, 51]

$$P(\{\alpha_{\kappa,H}\}) = \prod_{\kappa} \frac{1}{\pi \langle n_{\kappa} \rangle} \exp \left(-\frac{|\alpha_{\kappa,H}|^2}{\langle n_{\kappa} \rangle} \right), \quad (3)$$

where $\alpha_{\kappa,H}$ are H-polarized coherent states, in the mode κ associated with the x component of the transverse wave vector, and $\langle n_{\kappa} \rangle$ is the corresponding average photon number, which is assumed for simplicity to be constant [50]. In this case, Eq. (1) reduces to [18]

$$G^{(2)}(x_p, x_q) = G^{(1)}(x_p)G^{(1)}(x_q) + |G^{(1)}(x_p, x_q)|^2, \quad (4)$$

where $G^{(1)}$ is the first-order correlation function (see Eq. 9). Therefore, the second-order correlation function $G^{(2)}(x_p, x_q)$ depends on two contributions: the first one, $G^{(1)}(x_p)G^{(1)}(x_q) \propto \langle n(x_p) \rangle \langle n(x_q) \rangle$, is a constant background; the second one, $|G^{(1)}(x_p, x_q)|^2 \propto \langle \Delta n(x_p) \Delta n(x_q) \rangle$, is the interesting part of the correlation. The background can be removed by performing a correlation measurement between the fluctuations of the number of photons [22]. The outcome of this measurement is different from zero for all the possible pairs of paths $(p, q) = (1_C, 1_T), (2_C, 2_T), (1_C, 2_T), (2_C, 1_T)$, provided the relative distance between each pair of pinholes is smaller than the transverse coherence length of the source (l_{coh}) on the plane of the masks, which is: $|x_p - x_q| \ll l_{coh}$. An interesting result comes out by working in the hypothesis that

- A. the corresponding pairs of pinholes of the two masks are within the transverse coherence length, which is

$$|x_{1_C} - x_{1_T}| \ll l_{coh} \quad |x_{2_C} - x_{2_T}| \ll l_{coh}; \quad (5)$$

B. the pinholes, in each mask, are separated by a distance larger than the transverse coherence length of the source, which, given the condition in Eq. (5), implies

$$|x_{1C} - x_{2T}| \gg l_{coh} \quad |x_{1T} - x_{2C}| \gg l_{coh}. \quad (6)$$

In fact, in this case, only the two pairs of paths $(1_C, 1_T)$ and $(2_C, 2_T)$, each one associated with two disjoint paths spatially coherent with respect to each other, contribute to the correlation, while no contribution comes from the two pairs of paths $(1_C, 2_T)$ and $(2_C, 1_T)$, namely

$$\langle \Delta n(x_p) \Delta n(x_q) \rangle \neq 0 \Leftrightarrow (p, q) = (1_C, 1_T), (2_C, 2_T). \quad (7)$$

Multi-photon correlations (“photon bunching”) thus give rise to the non-vanishing expectation value of the product of the photon-number fluctuations at the two remote pinholes 1_C and 1_T (or 2_C and 2_T). This result arises from the correlation measurement and cannot be explained in terms of independent measurements at the two detectors. Interestingly, since the detectors are placed in the mask planes, the two pairs of disjoint paths $(1_C, 1_T)$ and $(2_C, 2_T)$ contribute independently of one another to the correlation measurement.

What happens if we perform correlation measurements after the two-pinhole masks? Since light passing through the two pinholes of each mask is incoherent (condition in Eq. 6), one may expect that the two contributions $(1_C, 1_T)$ and $(2_C, 2_T)$ add incoherently. However, as we shall show, they give rise to a counterintuitive spatial interference effect. To demonstrate this result we evaluate the correlation between the photon-number fluctuations $\Delta n(x_C)$ and $\Delta n(x_T)$ measured at equal detection times by the detectors D_C and D_T , respectively, placed at the transverse position x_C and x_T behind the two-pinhole masks, namely

$$\langle \Delta n(x_C) \Delta n(x_T) \rangle \propto |G^{(1)}(x_C, x_T)|^2. \quad (8)$$

Here,

$$G^{(1)}(x_C, x_T) = \text{Tr}[\hat{\rho}_H \hat{E}_C^{(-)}(x_C) \hat{E}_T^{(+)}(x_T)] \quad (9)$$

is the first-order correlation function calculated at x_C, x_T , where $\hat{E}_d^{+}(x_d)$ and $\hat{E}_d^{-}(x_d)$ are, respectively, the positive and negative frequency part of the electric field operator at the position x_d , namely

$$\hat{E}_d^{(+)}(x_d) = K \int d\kappa g\{\kappa; S, x_d\} \hat{a}_S(\kappa), \quad (10)$$

where K is a constant and $g\{\kappa; S, x_d\}$ is the Green’s function that describes the propagation of the mode κ from the source S to the detector D_d , placed in x_d , with $d = C, T$, and $\hat{a}_S(\kappa)$ is the annihilation operator at the source S associated with the mode κ .

As demonstrated in Appendix B, in the paraxial approximation and by using the conditions given in Eqs. (5) and (6), Eq. (8) becomes

$$\langle \Delta n(x_C) \Delta n(x_T) \rangle \propto |G_{1_C, 1_T}^{(1)}(x_C, x_T) + G_{2_C, 2_T}^{(1)}(x_C, x_T)|^2, \quad (11)$$

where $G_{1_C, 1_T}^{(1)}$ and $G_{2_C, 2_T}^{(1)}$ indicate the contributions to the correlation measurement coming from the two pairs of disjoint paths $(1_C, 1_T)$, $(2_C, 2_T)$, respectively, and, as shown in Appendix A,

$$G_{p,q}^{(1)}(x_C, x_T) \propto B_p^*(x_C) B_q(x_T) FT \{ |A(x_S)|^2 \} [(x_p - x_q)/(\lambda z)], \quad (12)$$

with the two phase factors $B_p^*(x_C)$ and $B_q(x_T)$ defined in Eq. (31) and the Fourier transform $FT \{ |A(x_S)|^2 \} [\chi]$ of the source intensity profile $|A(x_S)|^2$ calculated at $\chi = (x_p - x_q)/(\lambda z)$. The result of Eq. (12) is at the core of the counterintuitive interference phenomenon addressed in this paper. In fact, it indicates that the contributions $G_{p,q}^{(1)}$, associated with the pairs of paths $(p, q) = (1_C, 1_T), (2_C, 2_T), (1_C, 2_T), (2_C, 1_T)$, strongly depend on the relative distance $x_p - x_q$ between the remote pinholes p (of mask C) and q (of mask T) as compared to the transverse coherence length of the source (l_{coh}) on the plane of the masks. In our scenario, due to the conditions given in Eqs. (5) and (6), we obtain

$$\begin{aligned} G_{1_C, 1_T}^{(1)}(x_C, x_T) &\propto B_{1_C}^*(x_C) B_{1_T}(x_T) \quad , \quad G_{2_C, 2_T}^{(1)}(x_C, x_T) \propto B_{2_C}^*(x_C) B_{2_T}(x_T) \\ G_{1_C, 2_T}^{(1)}(x_C, x_T) &= G_{2_C, 1_T}^{(1)}(x_C, x_T) = 0. \end{aligned} \quad (13)$$

Table 1: Summary of the conditions for monitoring the transverse spatial structure and position of two remote double-pinhole masks by performing the correlation measurement of Eq. (14) in the setup in Fig. 1. In each of the five experimental scenarios one variable parameter is monitored, and the other parameters are fixed in order to “magnify” the effect of small variations of the monitored parameter; the corresponding “magnification” factors are reported in the third column of the table.

Experimental conditions in addition to Eqs. (5) and (6)	Variable parameter to monitor	“Magnification” factors
(i) $x_T = x_C, s_T = s_C$	$d_T - d_C$	$s_C/h - x_C/f$
(ii) $x_T = -x_C, s_T = -s_C$	$d_T + d_C$	$-s_C/h + x_C/f$
(iii) $ s_T \neq s_C $	$d_{T,C}$	$s_{T,C}/h - x_{T,C}/f$
(iv) $d_T = d_C$	$s_T - s_C$	d_C/h
(v) $d_T \neq d_C$	$s_{T,C}$	$d_{T,C}/h$

Therefore, as reported in Eq. (11), the correlation between the fluctuations of the number of photons enables to retrieve the *interference* between the two possible “photon bunching” contributions $G_{1_C,1_T}$ and $G_{2_C,2_T}$ associated with the pairs of disjoint paths $(1_C, 1_T)$ and $(2_C, 2_T)$. In fact, these two contributions add coherently and cannot be distinguished in the correlation measurement. As mentioned above, these two contributions can be distinguished when performing correlation measurements on the mask planes. In this case, these two contributions lead to independent bunching events due to both the statistical properties of the chaotic source and the experimental conditions in Eqs. (5) and (6). In contrast, when correlation measurements are performed after the two masks, the two pairs of path $(1_C, 1_T)$ and $(2_C, 2_T)$ become *indistinguishable*. Multi-photon correlations emerge from the resulting interference between the two pairs of disjoint paths, even if the pinholes in each mask are separated much further than the coherence length of the source.

3 Sensing applications

As shown in Appendix B, the correlation in the fluctuation of the number of photons in Eq. (11) can be written as

$$\langle \Delta n(x_C) \Delta n(x_T) \rangle \propto |1 + e^{i\phi(s_C, d_C, s_T, d_T, x_C, x_T)}|^2, \quad (14)$$

with

$$\phi(s_C, d_C, s_T, d_T, x_C, x_T) = \frac{2\pi}{\lambda} \left(\frac{s_T d_T - s_C d_C}{h} - \frac{x_T d_T - x_C d_C}{f} \right), \quad (15)$$

where h is defined by the condition $1/h = 1/z + 1/f$, $d_j := x_{2_j} - x_{1_j}$ is the pinhole separation for the j -th mask and $s_j := (x_{1_j} + x_{2_j})/2$ is the transverse coordinate of the center of the j -th mask, with $j = C, T$. Remarkably, the interference effect described by Eq. (14) holds for any value of the parameters z and f , namely, for any distance of the masks from the beam splitter and from the corresponding detectors.

Interestingly, for a fixed wavelength λ , the phase $\phi(s_C, d_C, s_T, d_T, x_C, x_T)$ is determined by the pinhole separations d_C and d_T weighted either by the average transverse positions s_j of the two pinholes divided by h , or by the detection angles x_j/f evaluated with respect to the optical axis. Therefore, the correlation measurement of Eq. (14) is sensitive to the position and the transverse structure of the two masks.

In Table 1, we consider five different experimental scenarios exploiting correlation measurement for monitoring small variations in: (i) the difference $d_C - d_T$ of the two pinhole separations, (ii) the sum $d_C + d_T$ of the two pinhole separations, (iii) the pinhole separation d_j in one mask $j = C, T$ if the separation in the other mask is fixed, (iv) the relative position $s_T - s_C$ of the masks, (v) the transverse position s_j of one mask $j = C, T$ if the position of the other mask is fixed. Interestingly, as reported in the third column of Table 1, in all scenarios it is possible to increase the precision of the measurement without either increasing the frequency of the light or using entanglement: the trick is to employ the remaining spatial parameters to “magnify” the effect of the variation of the spatial parameter to be monitored. An analysis of the sensitivity of this technique in terms of the number of resources is beyond the scope of this paper and will be addressed in future research [31].

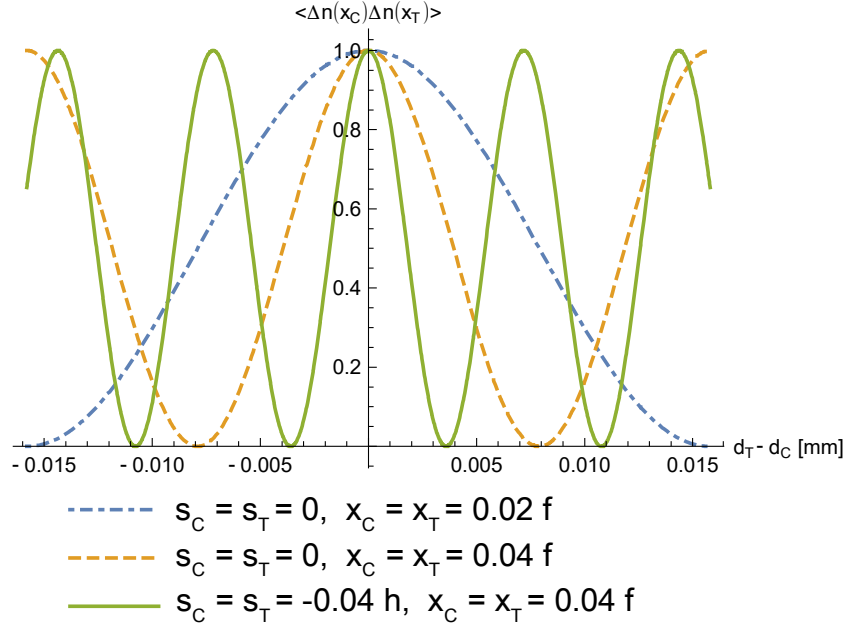


Figure 2: Simulation of the measurement of the stretching/shrinking $d_C - d_T$ of one mask with respect to the other in the setup of Fig. 1 with $z = 500\text{mm}$ and $f = 100\text{mm}$. The source is assumed to have a constant profile, with size $a = 2\text{mm}$, and wavelength $\lambda = 632\text{nm}$, so that the coherence length is $l_{coh} = \lambda z/a = 0.158\text{mm}$. When the two pinholes in each mask are placed symmetrically with respect to the optical axis ($s_C = s_T = 0$), the observable effect of small variations in $d_C - d_T$ is enhanced when the transverse position $x_C = x_T$ of the two detectors is increased, as demonstrated by the dashed (yellow) curve as compared to the dash-dot (blue) one. A further enhancement is obtained by displacing equally both masks with respect to the optical axis in the opposite direction of the detectors, as demonstrated by the continuous (green) curve.

In Fig. 2, we depict the first experimental scenario reported in Table 1, where, for equal transverse positions $s_C = s_T$ of the two masks, the correlation measurement at equal detector positions $x_C = x_T$ is sensitive to the stretching/shrinking $d_C - d_T$ of one mask with respect to the other. In the simple case where the two pinholes in each mask are placed symmetrically with respect to the optical axis ($s_C = s_T = 0$), the effect of small variations in $d_C - d_T$ can be magnified by moving both detectors at larger angles x_C/f with respect to the optical axis (dashed yellow curve). A further enhancement can be obtained by displacing both masks equally with respect to the optical axis, but in the opposite direction of the detectors (green continuous curve).

Based on Eqs. (14) and (15), the transverse structure of the two masks can also be retrieved, indirectly, by measuring the period of the second-order interference pattern $\langle \Delta n(x_C) \Delta n(x_T) \rangle$ obtained in the experimental scenarios reported in Table 2. For example, by performing correlation measurements at both equal and opposite positions with respect to the optical axis (first and second experimental scenarios, respectively, in Table 2) it is possible to retrieve the pinhole separations d_C and d_T in each mask.

Interestingly, the sensing capabilities of the present interferometric technique have currently no counterparts in the temporal domain [11].

4 Simulation of quantum logic gates

In this section, we show that quantum logic operations can be simulated by using the spatial interference effect described so far. In particular, we address the simulation of a controlled- U_ϕ gate, with U_ϕ

Table 2: Summary of the experimental conditions for characterizing two remote double-pinhole masks by measuring in the setup in Fig. 1 the period of the second order interference pattern given by Eq. (14).

Experimental conditions in addition to Eqs. (5) and (6)	Experimental variable	Period of the interference pattern $\langle \Delta n(x_C) \Delta n(x_T) \rangle$
(i) $x_T = x_C$	x_C	$\lambda f / (d_C - d_T)$
(ii) $x_T = -x_C$	x_C	$\lambda f / (d_T + d_C)$
(iii) $s_T = s_C, x_C = x_T = 0$	$d_T - d_C$	$\lambda h / s_C$
(iv) $s_T = -s_C, x_C = x_T = 0$	$d_T + d_C$	$\lambda h / s_C$
(v) $d_T = d_C, x_C = x_T = 0$	$s_T - s_C$	$\lambda h / d_C$

described by the matrix [25]

$$U_\phi := \begin{pmatrix} 0 & e^{i\phi} \\ e^{i\phi} & 0 \end{pmatrix}. \quad (16)$$

Let us start by describing a *genuine* controlled- U_ϕ gate. Given two-qubit input states $|\phi_C\rangle_C |\phi_T\rangle_T$, where

$$|\phi_C\rangle_C := \cos \phi_C |H\rangle_C + \sin \phi_C |V\rangle_C, \quad (17)$$

and

$$|\phi_T\rangle_T := \cos \phi_T |H\rangle_T + \sin \phi_T |V\rangle_T, \quad (18)$$

the controlled- U_ϕ gate operates on the input states, by giving the following output entangled state [25]

$$|\psi\rangle = \cos \phi_C |H\rangle_C |\phi_T\rangle_T + e^{i\phi} \sin \phi_C |V\rangle_C |\phi_T^{(F)}\rangle_T, \quad (19)$$

where

$$|\phi_T^{(F)}\rangle_T := \sin \phi_T |H\rangle_T + \cos \phi_T |V\rangle_T. \quad (20)$$

The polarization-dependent joint detection probability associated with the state $|\psi\rangle$ is [25]

$$P_{U_\phi} := |\langle \theta_C, \theta_T | \psi \rangle|^2 = \left| \cos \phi_C \cos \theta_C \cos (\phi_T - \theta_T) + e^{i\phi} \sin \phi_C \sin \theta_C \sin (\phi_T + \theta_T) \right|^2. \quad (21)$$

In particular, for $\phi = 0$, the controlled- U_ϕ gate reduces to a CNOT gate [25] and the polarization-dependent joint detection probability in Eq. (21) becomes

$$P_{\text{CNOT}} := |\langle \theta_C, \theta_T | \psi \rangle|^2 = \left| \cos \phi_C \cos \theta_C \cos (\phi_T - \theta_T) + \sin \phi_C \sin \theta_C \sin (\phi_T + \theta_T) \right|^2. \quad (22)$$

In order to simulate a controlled- U_ϕ gate we propose in Fig. 3 a modification of the interferometer in Fig. 1. The interferometer consists of three parts: the first one prepares the initial polarization state in the “control” input port \mathcal{C} and in the “target” input port \mathcal{T} ; the second one implements polarization transformations along the control and target output channels; the final part consists of the measurement process.

In the first part of the setup, the H-polarized chaotic light impinges on a balanced non-polarizing beam splitter and then propagates through two half-wave plates R_{ϕ_C} and R_{ϕ_T} .

The second part of the setup consists of a “control” path, connecting the ports \mathcal{C} and C , and a “target” path, connecting the ports \mathcal{T} and T . Similar to the setup in Fig. 1, both in the control and in the target paths light goes through identical two-pinhole masks. However, in the control path, two polarizers oriented along the H and V directions are placed just before pinholes 1_C and 2_C , respectively, while in the target path a half-wave plate oriented at $\pi/4$ is placed just before the pinhole 2_T .

Let us now describe the detection process. A polarizer, oriented along the direction $\theta_d := (\cos \theta_d \quad \sin \theta_d)^T$, with $d = C, T$, is placed in front of each detector. A polarization-dependent correlation measurement between the fluctuations of the number of photons $\Delta n(x_C, \theta_C)$ and $\Delta n(x_T, \theta_T)$, detected, respectively, by D_C and D_T , is then performed.

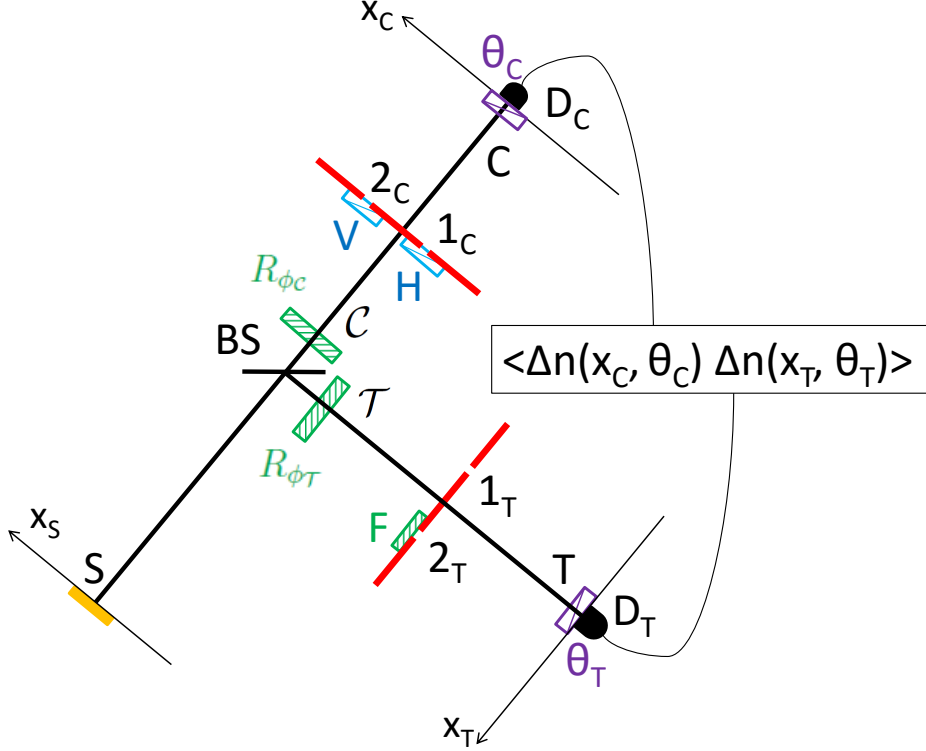


Figure 3: Interferometer for the simulation of controlled- U_ϕ gates, with U_ϕ defined in Eq. (16). In the first part of the interferometer, the initial polarization state of the light is prepared. The second part, from the ports \mathcal{C} and \mathcal{T} to the ports C and T , respectively, performs a polarization-dependent transformation. Correlation measurements in the fluctuations of the number of photons are performed at the interferometer output. R_{ϕ_C} and R_{ϕ_T} are two half-wave plates that rotate the polarization of the angles ϕ_C and ϕ_T , respectively; F is a half-wave plate implementing a flip from the horizontal (H) polarization to the vertical (V) polarization and vice versa; H , V , θ_C and θ_T represent the polarization directions of the corresponding polarizers.

As shown in Appendix C, if the conditions in Eqs. (5) and (6) are satisfied, in the paraxial approximation the correlation between the fluctuations of the number of photons is proportional to the joint detection probability typical of a controlled- U_ϕ gate, namely

$$\langle \Delta n(x_C, \theta_C) \Delta n(x_T, \theta_T) \rangle \propto \left| G_{1_C, 1_T}^{(1)}(x_C, \theta_C, x_T, \theta_T) + G_{2_C, 2_T}^{(1)}(x_C, \theta_C, x_T, \theta_T) \right|^2 \propto P_{U_\phi}, \quad (23)$$

with ϕ defined in Eq. (15). However, differently from the setup in Fig. 1, the two interfering contributions $G_{1_C, 1_T}^{(1)}$ and $G_{2_C, 2_T}^{(1)}$, associated with the propagation through the two pairs of pinholes $(1_C, 1_T)$ and $(2_C, 2_T)$, are polarization dependent. In particular:

- A. the control path 1_C , associated with the polarization mode H, is correlated with the target path 1_T , where the polarization is not modified;
- B. the control path 2_C , associated with the polarization mode V, is correlated with the target path 2_T , where the polarization is flipped from H to V, and vice versa.

Interestingly, the resulting second-order interference pattern is proportional to the probability P_{U_ϕ} associated with a controlled- U_ϕ gate, with ϕ defined in Eq. (15). In particular, when

$$|\phi(s_C, d_C, s_T, d_T, x_C, x_T)| \ll 1, \quad (24)$$

Eq. (23) reduces to

$$\langle \Delta n(x_C, \theta_C) \Delta n(x_T, \theta_T) \rangle \propto P_{CNOT}, \quad (25)$$

with P_{CNOT} defined in Eq. (22), leading to the *simulation* of a CNOT gate operation without recurring to any entanglement processes.

Based on Eq. (15), the condition reported in Eq. (24) can be experimentally obtained, for example, by performing the detections at equal positions $x_C = x_T$ with the pinholes in the two masks placed in the same position with respect to the optical axis ($d_C = d_T$, $s_C = s_T$).

By using a generalized N-port beam splitter and N double-slit masks, the scheme in Fig. 3 can be generalized for the simulation of interference features typical of N-order entangled correlations.

5 Discussions

Based on the setup in Fig. 1, we have theoretically demonstrated a second-order spatial interference effect between two pairs of disjoint but correlated paths. The two interfering paths are associated with the pairs of remote pinholes $1_C, 1_T$ and $2_C, 2_T$. Interestingly, such interference exists even if the pinholes in each mask are separated by a distance much larger than the transverse coherence length l_{coh} of the source. In fact, the interference between the pairs of paths $(1_C, 1_T)$ and $(2_C, 2_T)$ arises from the correlation between the two disjoint paths going through pinholes $1_C, 1_T$ and $2_C, 2_T$, respectively; in fact, the transverse distance between the two pinholes 1_C and 1_T (or 2_C and 2_T) is smaller than the transverse coherence length of the source. This is not the case for the other two possible pairs of paths, $(1_C, 2_T)$ and $(2_C, 1_T)$, which therefore cannot contribute to the interference. This phenomenon, substantially different from all second-order interference phenomena based on multiple chaotic sources [40, 41, 42, 43], thus provides a deeper understanding of the physics of multi-path interference and spatial coherence.

Furthermore, we have demonstrated that this spatial interference effect has interesting potential applications for sensing of remote objects in the absence of first-order coherence. In particular, we have shown that information about both the transverse structure and the relative position of two remote double-pinhole masks is encoded within the relative phase between the two interfering pairs of optical paths (Eq. (15)). These spatial parameters can be retrieved through the measurement of the period of the second order interference pattern given by Eq. (14) (Table 2). Remarkably, the effect produced on the correlation measurement by small variations of these spatial parameters can be enhanced without increasing the frequency of the light, as demonstrated in Table 1 and in the example in Fig. 2. This may lead to novel applications in sensing biological samples without exposure to high-frequency light [52]. Moreover, this technique can be applied independently of the distances between the two masks and the source and between the masks and the corresponding detectors. Therefore, this effect can be potentially employed for monitoring the relative spatial structure and position of distant objects.

In addition, we have demonstrated how to exploit this novel spatial interference phenomenon for simulating entanglement correlations, including the simulation of a CNOT gate (Fig. 3). This technique can be used, to simulate typical interference features of high-order entanglement correlations with potential applications in novel optical algorithms [53, 54, 55, 56, 57, 58].

In conclusion the proposed spatial interference effect provides a deeper understanding of the physics of spatial coherence and multi-photon interference, and can naturally lead to novel interferometric techniques for sensing distant objects and simulating small-scale quantum circuits. This interference phenomenon may also be extended to atomic interferometers with thermal bosons, for example, to measure the effect of external forces (e.g., gravity) on bosons of given mass in remote spatial regions.

A Green's propagator for the setup in Fig. 1

Given the optical setup in Fig. 1 we calculate here the Green's propagator $g\{\kappa; S, x_d\}$, associated with the x component κ of transverse wave-vector, from the source S with amplitude profile $A(x_S)$ to the detector transverse position x_d , with $d = C, T$. In particular, we obtain [18, 59, 60]

$$\begin{aligned}
g\{\kappa; S, x_d\} &= \frac{1}{\sqrt{2}} e^{i\varphi(d)} \int dx_S dx_M A(x_S) M(x_M) e^{i\kappa x_S} \left\{ \frac{-i\omega}{2\pi c} \frac{e^{i\omega z/c}}{z} \mathcal{G}(|x_S - x_M|)_{[\omega/(cz)]} \right\} \\
&\times \left\{ \frac{-i\omega}{2\pi c} \frac{e^{i\omega f/c}}{f} \mathcal{G}(|x_M - x_d|)_{[\omega/(cf)]} \right\}, \tag{26}
\end{aligned}$$

where ω is the frequency of the light,

$$M(x_M) := \sum_{x_p} \delta(x_M - x_p) \quad (27)$$

is the mask transfer function, defined by the transverse position x_p of the pinholes $p = 1_C, 2_C$ for the upper mask and $p = 1_T, 2_T$ for the lower mask,

$$\mathcal{G}(|\alpha|)_{[\beta]} := e^{i\frac{\beta}{2}|\alpha|^2} \quad (28)$$

is the Fresnel propagator, and the factor $\frac{1}{\sqrt{2}}e^{i\varphi(d)}$ takes into account the propagation through the beam splitter, with $\varphi(C) = 0$ for the transmitted beam and $\varphi(D) = \pi/2$ for the reflected beam.

By using the definition (28) and the property

$$\mathcal{G}(|\alpha + \alpha'|)_{[\beta]} = \mathcal{G}(|\alpha|)_{[\beta]} \mathcal{G}(|\alpha'|)_{[\beta']} e^{i\beta\alpha\alpha'} \quad (29)$$

of the Fresnel propagator, and the mask transfer function in Eq. (27), Eq. (26) becomes

$$g\{\kappa; S, x_d\} = \sum_{p=1_d, 2_d} B_j(x_d) \int dx_S A(x_S) \mathcal{G}(|x_S|)_{[\omega/(cz)]} e^{i[\kappa - \omega x_p/(zc)]x_S}, \quad (30)$$

where

$$B_p(x_d) := -\frac{1}{\sqrt{2}} \left(\frac{\omega}{2\pi c} \right)^2 \frac{e^{i[\varphi(d) + \omega(z+f)/c]}}{zf} \mathcal{G}(|x_d|)_{[\omega/(cf)]} \mathcal{G}(|x_p|)_{[\omega/(ch)]} e^{-i\omega x_d x_p/(fc)}. \quad (31)$$

The Green's function in Eq. (30) can be finally written as the sum

$$g\{\kappa; S, x_d\} = \sum_{p=1_d, 2_d} g_p\{\kappa; S, x_d\}, \quad (32)$$

of the two Green's propagators

$$g_p\{\kappa; S, x_d\} := B_p(x_d) \int dx_S A(x_S) \mathcal{G}(|x_S|)_{[\omega/(cz)]} e^{i[\kappa - \omega x_p/(zc)]x_S}, \quad (33)$$

from the source S to the detector position x_d , with $d = C, T$, through the pinhole located in x_p , with $p = 1_d, 2_d$.

B Correlation measurement for the setup in Fig. 1

In the present appendix we present a detailed derivation of the correlation in the fluctuation of the numbers of photons in Eqs. (11) and (14) measured at the output of the setup in Fig.1.

By substituting in Eq. (9), the definition of the electric field operator (Eq. (10) with the Green's propagator in Eq. (32), we obtain the first order correlation function

$$G^{(1)}(x_C, x_T) = \sum_{\substack{p=1_C, 2_C \\ q=1_T, 2_T}} |K|^2 \text{Tr} \left[\hat{\rho}_H \int d\kappa d\kappa' g_p^*\{\kappa; S, x_C\} g_q\{\kappa'; S, x_T\} \hat{a}_S^\dagger(\kappa) \hat{a}_S(\kappa') \right]. \quad (34)$$

This expression corresponds to the sum

$$G^{(1)}(x_C, x_T) = \sum_{\substack{p=1_C, 2_C \\ q=1_T, 2_T}} G_{p,q}^{(1)}(x_C, x_T). \quad (35)$$

of the four contributions

$$G_{p,q}^{(1)}(x_C, x_T) := |K|^2 \text{Tr} \left[\hat{\rho}_H \int d\kappa d\kappa' g_p^*\{\kappa; S, x_C\} g_q\{\kappa'; S, x_T\} \hat{a}_S^\dagger(\kappa) \hat{a}_S(\kappa') \right], \quad (36)$$

from the corresponding four pairs of optical paths $(p, q) = (1_C, 1_T), (2_C, 2_T), (1_C, 2_T), (2_C, 1_T)$.

By using the property of chaotic sources [50]

$$\text{Tr} [\hat{\rho} a^\dagger(\kappa) a(\kappa')] = \langle n_\kappa \rangle \delta(\kappa - \kappa'), \quad (37)$$

where the average photon number $\langle n_\kappa \rangle$ in the mode κ is assumed to be constant, and the Green's propagators in Eq. (33), Eq. (36) reduces to

$$G_{p,q}^{(1)}(x_C, x_T) = K' B_p^*(x_C) B_q(x_T) FT \{ |A(x_S)|^2 \} [\omega(x_p - x_q)/(2\pi cz)], \quad (38)$$

where $K' := |K|^2 \langle n_\kappa \rangle$ and $FT \{ |A(x_S)|^2 \} [\chi]$ represents the Fourier transform of the source intensity profile, calculated in $\omega(x_p - x_q)/(2\pi cz)$. If $|x_p - x_q| \gg l_{coh}$, this Fourier transform is approximately zero, so that no contribution to the correlation function in Eq. (35) arises from the pair of paths (p, q) . On the contrary the pair of path (p, q) gives its maximum contribution if $|x_p - x_q| \ll l_{coh}$. This implies that, in the conditions given in Eqs. (5) and (6), the correlation function in Eq. (35) reduces to the sum

$$G^{(1)}(x_C, x_T) = G_{1_C, 1_T}^{(1)}(x_C, x_T) + G_{2_C, 2_T}^{(1)}(x_C, x_T) \quad (39)$$

of the only two contributions associated with the pairs of paths $(1_C, 1_T)$ and $(2_C, 2_T)$. By substituting this expression in Eq. (8), we obtain the correlation in the photon-number fluctuations $\langle \Delta n(x_C) \Delta n(x_T) \rangle$ in Eq. (11).

By using the conditions in Eqs. (5) and (6) and Eq. (38), Eq. (11) can be written explicitly as

$$\langle \Delta n(x_C) \Delta n(x_T) \rangle = |K' FT \{ |A(x_S)|^2 \} (0) [B_{1_C}^*(x_C) B_{1_T}(x_T) + B_{2_C}^*(x_C) B_{2_T}(x_T)]|^2. \quad (40)$$

By inserting the expressions in Eq. (31) with the definition of the Fresnel propagator (Eq. (28)), we finally obtain

$$\begin{aligned} \langle \Delta n(x_C) \Delta n(x_T) \rangle &= K'' |e^{-i\omega/(2ch)(x_{1_C}^2 - x_{1_T}^2)} e^{i\omega/(cf)(x_C x_{1_C} - x_T x_{1_T})} \\ &+ e^{-i\omega/(2ch)(x_{2_C}^2 - x_{2_T}^2)} e^{i\omega/(cf)(x_C x_{2_C} - x_T x_{2_T})}|^2, \end{aligned} \quad (41)$$

with $K'' := |(i/2) [1/(zf)]^2 K' [\omega/(2\pi c)]^4 FT \{ |A(x_S)|^2 \} (0)|^2$, which reduces easily to Eq. (14).

C Correlation measurement for the setup in Fig. 3

In the present appendix we derive the correlation in the fluctuations of the number of photons in Eq. (23), measured at the output of the interferometer in Fig. 3 for arbitrary polarization angle θ_C and θ_T . For a H-polarized quasi-monochromatic 1-dim chaotic source (thermal state $\hat{\rho}_H$ in Eq. (2)), this correlation is given by [3]

$$\langle \Delta n(x_C, \theta_C) \Delta n(x_T, \theta_T) \rangle = |G^{(1)}(x_C, \theta_C; x_T, \theta_T)|^2 \quad (42)$$

where

$$\begin{aligned} G^{(1)}(x_C, \theta_C; x_T, \theta_T) &= \text{Tr} [\hat{\rho}_H \hat{\mathcal{E}}_{C,S}^{(-)}(x_C) \hat{\mathcal{E}}_{T,S}^{(+)}(x_T)] \\ &= K' \int d\kappa L_C^*(\kappa) L_T(\kappa), \end{aligned} \quad (43)$$

is the first-order correlation function determined by the field operator

$$\hat{\mathcal{E}}_{d,S}^{(+)}(x_d) := K \int d\kappa e^{-i\omega t} L_d(\kappa) \hat{a}_S^{(H)}(\kappa), \quad (44)$$

with $d = C, T$, where K is a constant factor, $K' := |K|^2 \langle n_\kappa \rangle$ and

$$L_C(\kappa) := \frac{1}{\sqrt{2}} [g_{1_C} \{ \kappa; S, x_C \} \cos \theta_C \cos \phi_C + g_{2_C} \{ \kappa; S, x_C \} \sin \theta_C \sin \phi_C], \quad (45)$$

$$L_T(\kappa) := \frac{i}{\sqrt{2}} [g_{1_T} \{ \kappa; S, x_T \} \cos(\theta_T - \phi_T) + g_{2_T} \{ \kappa; S, x_T \} \sin(\theta_T + \phi_T)] \quad (46)$$

are the effective propagation functions. By substituting the expressions in Eqs. (45) and (46), the correlation function in Eq. (43) becomes

$$\begin{aligned}
G^{(1)}(x_C, \theta_C; x_T, \theta_T) = \frac{i}{2} K' \int d\kappa \Big[& \cos \theta_C \cos \phi_C \cos(\theta_T - \phi_T) g_{1_C}^* \{\kappa; S, x_C\} g_{1_T} \{\kappa; S, x_T\} \\
& + \sin \theta_C \sin \phi_C \sin(\theta_T + \phi_T) g_{2_C}^* \{\kappa; S, x_C\} g_{2_T} \{\kappa; S, x_T\} \\
& - \cos \theta_C \cos \phi_C \sin(\theta_T + \phi_T) g_{1_C}^* \{\kappa; S, x_C\} g_{2_T} \{\kappa; S, x_T\} \\
& - \sin \theta_C \sin \phi_C \cos(\theta_T - \phi_T) g_{2_C}^* \{\kappa; S, x_C\} g_{1_T} \{\kappa; S, x_T\} \Big]. \quad (47)
\end{aligned}$$

By using the result in Eq. (38) and by applying the conditions given in Eqs. (5) and (6) in an analogous way as in Appendix B, Eq. (47) reduces to Eq. (23).

Funding

M.C. acknowledges a Ph.D. studentship from the University of Bari. M.C., M. D. and A.G. acknowledge funding from P.O.N. RICERCA E COMPETITIVITA' 2007-2013 - Avviso n. 713/Ric. del 29/10/2010, Titolo II - "Sviluppo/Potenziamento di DAT e di LPP" (project n. PON02-00576-3333585). V.T. acknowledges the support of the German Space Agency DLR with funds provided by the Federal Ministry of Economics and Technology (BMWi) under grant no. DLR 50 WM 1556

Acknowledgments

M.C. is thankful for the hospitality of Prof. W. P. Schleich during his visit in the summer of 2015 at the Institute of Quantum Physics, Ulm University. M.C. and V.T. would also like to thank J. Seiler for useful discussions during this period.